Journal of Cultural Heritage 58 (2022) 209–218

Contents lists available at ScienceDirect

Journal of Cultural Heritage

journal homepage: www.elsevier.com/locate/culher

VSI: Geomaterials in CH

Coupling electrical resistivity methods and GIS to evaluate the effect of historic building features on wetting dynamics during wind-driven rain spells

Laura López-González[a], Miguel Gomez-Heras[b,*], Raquel Otero-Ortiz de Cosca[a], Soledad Garcia-Morales[c], Rafael Fort[d]

[a] Independent Architect
[b] Departamento de Geología y Geoquímica, Universidad Autónoma de Madrid, 28049, Madrid, Spain
[c] Departamento de Construcción y Tecnología Arquitectónica, Universidad Politécnica de Madrid, 28040, Madrid, Spain
[d] Instituto de Geociencias (CSIC-UCM), 28040, Madrid, Spain

ARTICLE INFO

Article history:
Received 1 April 2022
Accepted 11 October 2022

Key words:
Stone decay
Electrical resistivity tomography
Geographic information
Systems
4D mapping
Hydrometeorological anisotropy

ABSTRACT

Moisture is one of the most important factors causing building stone decay and rain penetration is one of the leading factors. Particularly, wind-driven rain spells, which are becoming increasingly common and seasonal as a result of climate change. Historic buildings' sometimes intricate design features can be a factor multiplying meteorological anisotropy, either shielding walls or increasing the surface that is affected by wind-driven rain spells. This paper aims to identify the effect of pilasters and tower buttresses on the wetting dynamics of a listed 9th Century historic building during a rain spell by means of electrical resistivity methods coupled with GIS mapping, paying special attention to how data representation and map algebra can improve the interpretation of several data sets of non-destructive testing. Results show how building features can modify deeply moisture dynamics and maximise local anisotropy. In the present case, a compound of an external tower buttress and an internal pilaster decreases moisture ingress through ground infiltration while increasing moisture retention into the wall due to its larger mass. This, in turn, multiplies the incidence of moisture-related processes inside the building. The presented data also highlight the usefulness of mapping over time (4D mapping) and of GIS to improve interpretations through map algebra.

1. Introduction

Moisture is one of the most important factors causing building stone decay. Wetting-drying cycles act directly dissolving, hydrolysing and transforming some of the rock constituents and, indirectly, influencing salt dissolution and crystallisation and biological decay. In addition to the material damage, moisture in masonry can, in turn, impact the safety, health, and comfort of the public occupying a certain building [1].

Therefore, there is a large body of research on the dynamics of both surface and deep-seated moisture on building stone and on wetting and drying dynamic and how it affects decay factors (e.g., [2–8]). The importance of recording moisture in historic buildings in the context of their conservation has been amply discussed (e.g., [9] and subsequent papers in the referred supplement) and even standardised (as discussed by Camuffo [10]). Particularly, the use of non-destructive techniques is crucial in assessing moisture in buildings. Besides being the preferable option in historical heritage buildings, they allow reiterating measurements, which is the only way to understand the dynamic evolution of moisture over time and, in due course, to take decisions of intervention [11]). Some of the non-destructive techniques used to assess moisture dynamics in building walls include thermo-hygrometric sensing (e.g., [12]), Infrared thermography (e.g., [13]), surface electrical resistance methods (e.g., [14]), Electrical Resistivity Tomography (e.g., [4,15,16]) Microwave and radar (e.g., [17]) or multi-technique approaches (e.g., [18–20]).

Amongst these non-destructive techniques, the present paper focuses on electrical resistivity methods to obtain an understand-

* Corresponding author.
E-mail address: miguel.gomezheras@uam.es (M. Gomez-Heras).

https://doi.org/10.1016/j.culher.2022.10.009

ing of both surface and subsurface moisture. Electrical resistivity methods are used to identify moisture based on the lower electrical resistivity wet materials have in relation to dry ones.

Electrical Resistivity Tomography (ERT) is a geophysical technique used to locate non-destructively subsurface wet areas in building walls by using non-invasive EKG electrodes [16,21-24]. Hand-held resistivity-based moisture meters give a single relative reading proportional to the amount of moisture in the outer portion of the material between the two metallic pins of the probe. Although many of these moisture meters (like the Protimeter Surveymaster used in this paper) are calibrated for wood, they are extensively used in other porous materials in built heritage studies. Although these techniques have some shortfalls quantifying absolute moisture (inasmuch salt content affects resistivity values), they are considered a good support tool for moisture investigations and their repeated use in a historic building during a wetting episode allow to visualise how moisture ingress is taking place [25,26].

All the previously referred techniques allow representing moisture data over space (i.e., mapping) and time, which is important to understand how moisture fronts evolve spatially during wetting. However, existing literature shows that mapping over time (e.g., [5,27]) is less common than single snapshots of moisture at a certain time, perhaps because, as Orr et al. [17] refer, this way of communicating results of measuring moisture in buildings is not formalised or standardised. One way of improving the results of mapping over time, as shown by previous research [12], is considering historic building walls as topographic surfaces and managing moisture and other measurements as "geographical" data in a GIS, which allows combining measurements and carrying out data operations and map algebra [28]. The use of GIS to represent and operate with non-destructive techniques results on stone building surfaces is a powerful, but surprisingly underused, methodology. The advancement of structure-from-motion and digital photogrammetry in recent years has facilitated this task, as they make possible obtaining topographic models at different scales suitable for stone weathering studies (e.g., [29–31]).

Rain penetration is arguably the leading factor, amongst the various sources found in historic buildings, for the presence of moisture in walls. Wind-driven rain spells deserve particular attention, as they modify the response of vertical walls to impinging rainwater [32] maximising the wetting and erosional effect of rain on walls and generating anisotropic decay of buildings and structures [33]. Short-term wind-driven spells associated to extreme hydrometeorological events are increasingly frequent and seasonal, as a result of climate change [34,35], which underlines the increasing concern on the threat Climate change poses to Cultural Heritage [36].

Historic buildings' design features, such as cornices, buttresses, etc. may be a factor multiplying meteorological anisotropy, either shielding walls or increasing the surface that can be wetted during a rain event, in addition to modifying moisture ingress through capillary suction or filtration. Pilasters or tower buttresses are a good example of these features, as they are attached to walls and modify locally the thickness affected by moisture.

2. Research aim

This study aims to identify the effect of pilasters and tower buttresses on the wetting dynamics of a 9th Century historic building during a rain spell by means of electrical resistivity methods (electrical resistivity tomography and surface electrical conductivity methods) coupled with GIS mapping, paying special attention to how data representation and map algebra can improve the interpretation of several data sets of non-destructive testing.

Table 1
Local times at which each set of measurements on the wall and the inside pilaster were taken during the 24 h survey.

		Local time	Rain
Day 1	Test 1	14:00–15:00	Yes
	Test 2	19:00–20:00	Yes
	Test 3	21:00–22:00	Yes
Day 2	Test 4	10:00–11:00	Yes
	Test 5	14:00–15:00	

3. Site description and methods

This study was carried out during a rain episode on the north wall of the church of the 9th Century Monastery of St Mary of Mave (Palencia, Spain). The Romanesque church of this Monastery was listed in the Spanish catalogue of protected goods of cultural interest in 1931 and it is the only part of the Monastery that preserves its original design (as the rest of the Monastery was transformed into a hotel). The church is a pseudobasilica with one common roof over the main nave and the lateral aisles (Fig. 1). The entrance (west) is covered by a portico and the south wall is attached to a cloister. Hence, only the three apses and the north wall can receive rainfall. The floor of the church is below the outside ground level, which favours the ingress of moisture from the outside unpaved ground into the church. The north wall has five attached tower buttresses (Fig. 2), which are thicker at the bottom than at the top. Three of the buttresses have corresponding pilasters attached to the internal wall. The church underwent several restorations between 1987 and 1989 and in 2006 due to moisture damage in roofs and walls [37]. None of these restorations included paving the grounds around the north wall of the church and since then moisture-related damage, including biological growth, has reappeared on the internal side of the north wall of the church.

The study was carried out in a 2.06 m high and 5.26 m wide portion of the internal side of the north wall (Figs. 1 and 2) including one of the internal pilasters which corresponds to one of the external tower buttresses. This area was selected as it showed the most noticeable moisture damage above the outside ground level and, particularly on the pilaster's surface.

The 1 m thick wall is constructed of two leaves of a local porous reddish Cretaceous sandstone with an unknown infill.

The church is in a warm-summer Mediterranean climate. The average air temperature recorded in the closest weather station of the national network (23 km away) in the month before the survey was 18.8 °C with a total precipitation of 31.4 mm and a prevailing north wind with an average velocity of 12 km/h (number 3 in Beaufort scale). The survey was made to coincide with a heavy rain in the early days of the month of June (which corresponds in average to the beginning of the decline of the rainy season). Specifically, the survey started the day of the heaviest rain (20.2 mm) within the preceding month. The rain was driven against the wall by a north wind (N11E) with average velocities between 11.6 and 17.3 km/h.

The survey was made across a 24 h interval beginning at mid-afternoon of the day heavy rain started and comprised 5 measurements (Table 1). The 3 first sets of measurements were made during day 1 (June 10th) with intermittent rain showers. The night between day 1 and 2 registered heavy rain throughout. Rain stopped on day 2 at 12:45 just after taking the fourth set of measurements. The last set of measurements was taken around 1–2 h after the rain stopped. Each set of measurements included: 1) point measurements with a hand-held moisture metre in resistivity mode, 2) profiles of electrical resistivity tomography (ERT) and 3) point

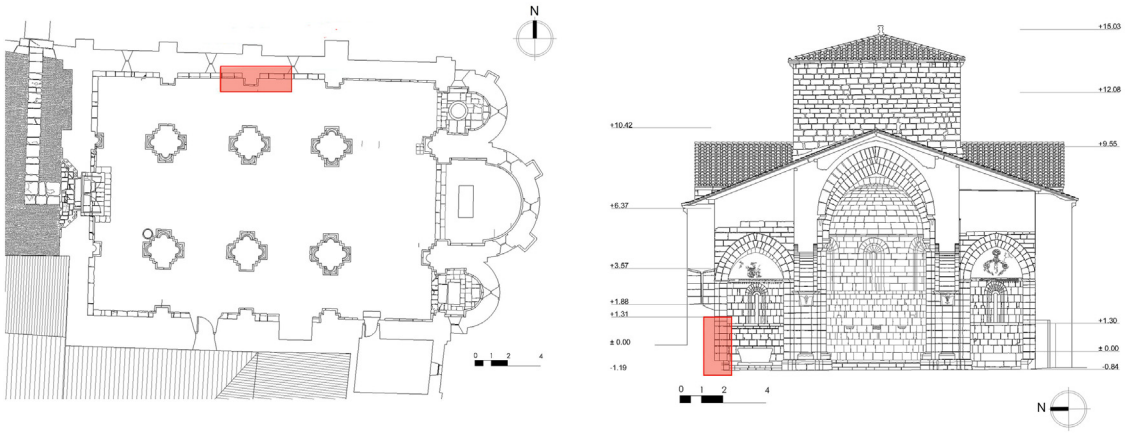

Fig. 1. Plan and section (looking towards the apse) of the church (after Nuño González et al. [37]). The red rectangle indicates the area surveyed in this study.

Fig. 2. Outside and inside view of the north wall of the church. The area surveyed in this study is marked in red. The level of the outside ground in the internal wall is marked with a yellow line.

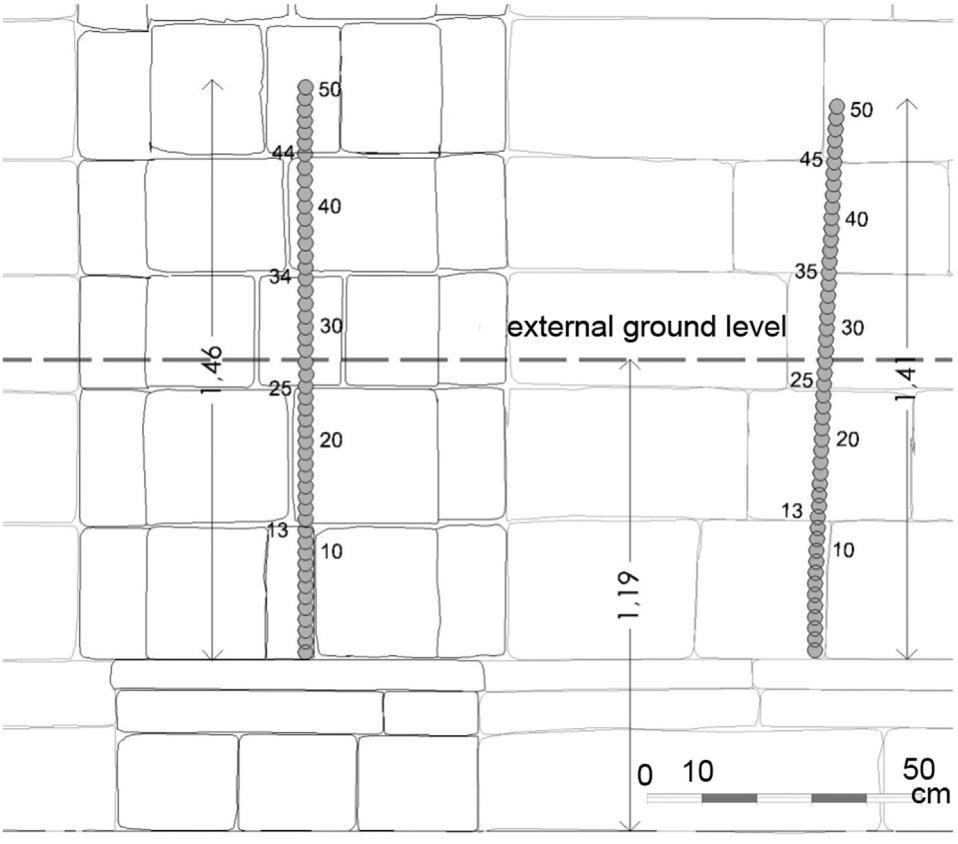

Fig. 3. Schematic view of the array of EKG sensors on the pilaster and the wall to obtain ERT profiles. The external ground level is marked with a dashed line for reference.

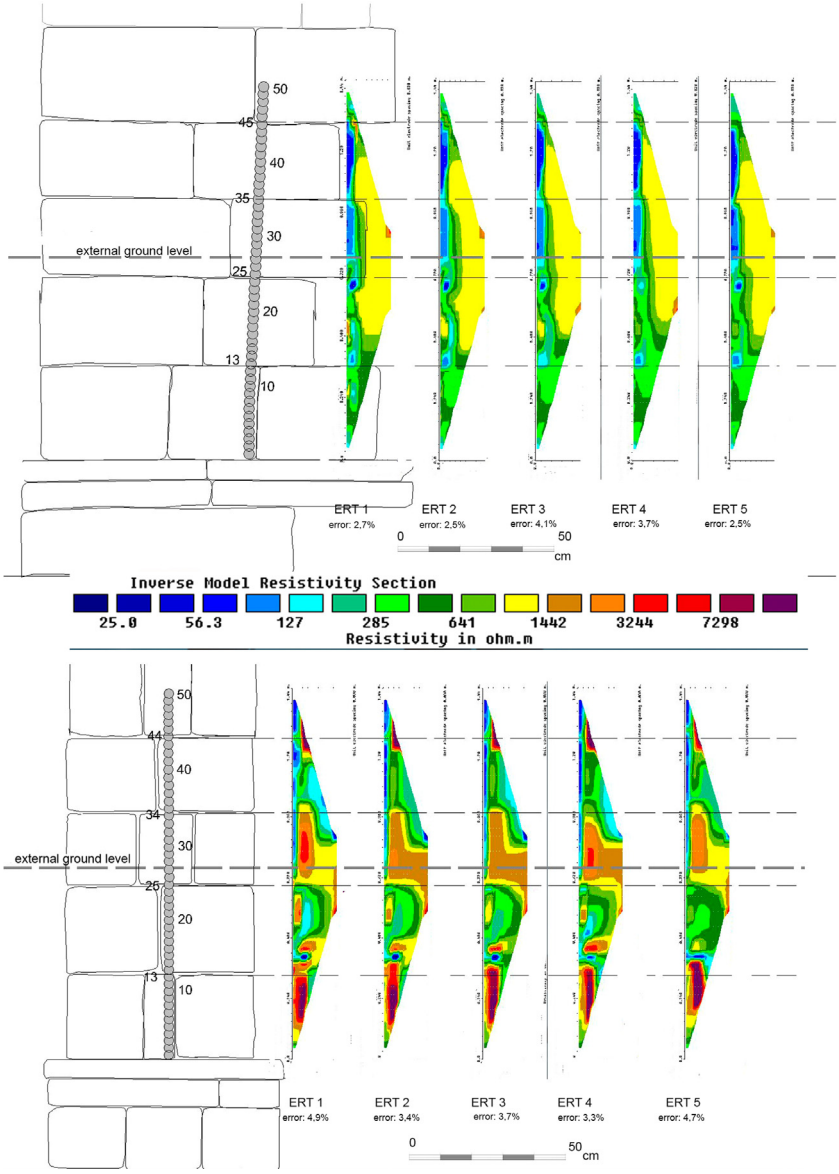

Fig. 4. Elevation view and ERT sections of the main portion of the wall (a) and of the pilaster (b) for the 5 different tests carried out at different times during the survey (see Table 1). ERT 1 to 3 correspond to day 1 and ERT 4 and 5 to day 2. The maximum depth of the sections is 24 cm (which corresponds to 1/6 of the section height). The figure shows how the areas with lower resistivity are related to joints between ashlars as well as to the surface. In the pilaster sections high resistivity areas are located at the very bottom of the sections and in the areas related to the external ground level. The error after the inversion is specified under each section.

hygrothermal inspection. The approximately 1-hour timespan for each set of measurements corresponds to the total time needed to carry out all these three types of tests.

Hand-held moisture metre measurements were made with a *GE Protimeter Surveymaster* in resistivity mode. A total of 303 wood moisture equivalent (%WME) readings were taken. Five measurements were taken on each of the blocks (at the centre and at the corners) plus four in each mortar joint between ashlars. The number of measurements was reduced in the blocks with smaller faces of the pilaster to three measurements on the block (one at the centre and two near the shorter sides) and two more on the mortar joints between rows.

ERT measurements were recorded with a GeoTomMK8E1000 Geolog 2000 equipment. Two vertical 1.44 m long profiles were recorded in each set of measurements using fifty 4 cm diameter *3 M Red Dot Micropore 2237* EKG sensors in each profile, one on the wall and one on the middle of the pilaster (Fig. 3). The bottom of the profile corresponded to the beginning of the flat area of the wall upon the 0.42 m plinth. The EKG sensors were placed with a slight overlap, so they were easier to remove after the tests. Therefore, their centres were at 3.7 cm. ERT profiles were obtained using a Wenner configuration [38].

A determination of the evaporation flow at different points was made to complement resistivity measurements, by means of a hygrothermal inspection with a digital thermos-hygrometer TESTO 610 recording air temperature (T) and dry bulb temperature (Td). The methodology developed by Garcia-Morales et al. [39] was used. This methodology seeks quantifying the level of evaporation at different points of a wall by comparing them with a so-called "intensity of evaporation factor" (F_i). Readings were taken by holding the thermo-hygrometer against the wall for each data point until the T and Td values stabilised (a few seconds). The values obtained with the thermo-hygrometer are converted into humidity ratios (W) in g/kg with a psychrometric chart. The outdoor humid-

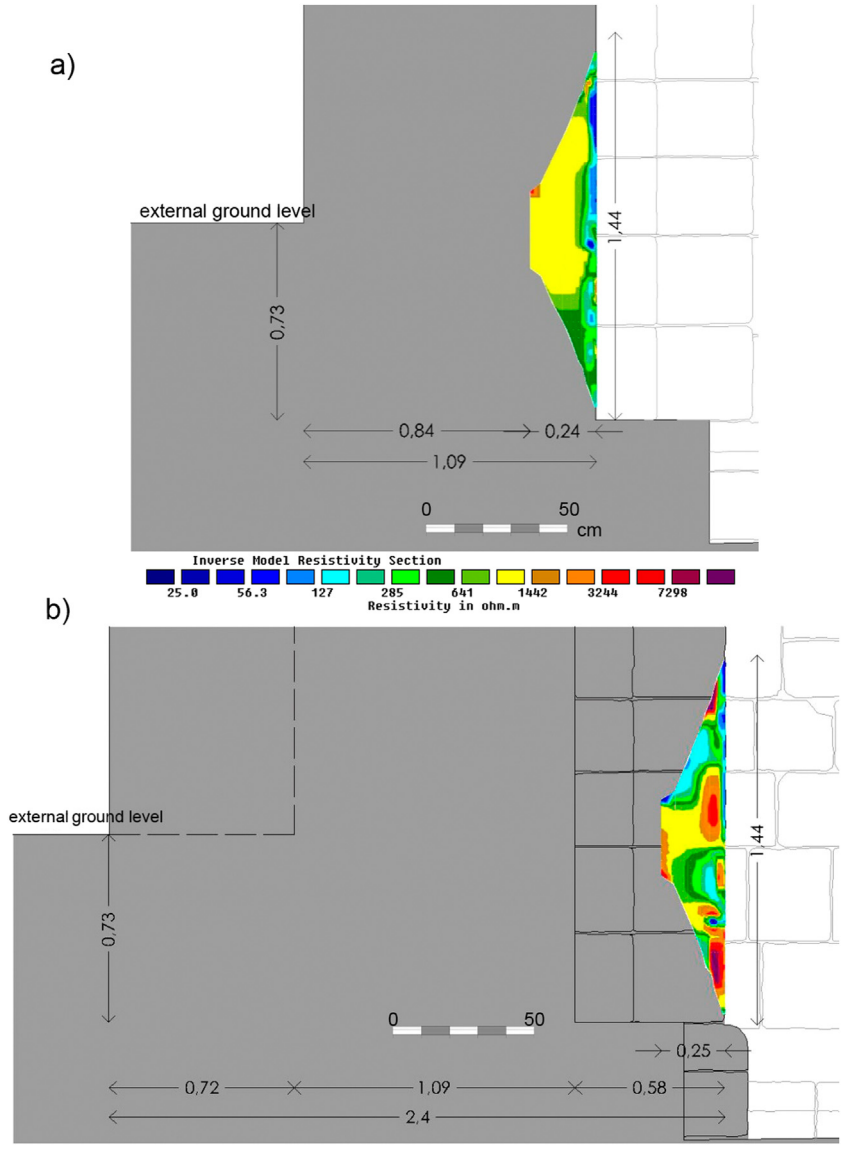

Fig. 5. Location of the ERT sections (ERT 1 is shown as an example) in a cross section of the full thickness of the main part of the wall (a) and the area where the outside buttress and the internal pilaster are located (b). Dimensions in the cross section are expressed in metres.

ity ratio (W_O) and the indoor humidity ratio (W_i) were also calculated for each of the tests.

The hygrothermal inspection does not quantify in itself the absolute flow of evaporation (mass of water per area) but it is a good approximation to the evaporation behaviour of the walls.

Hygrothermal measurements were taken in 148 points, one in the centre of each stone block in the surveyed area and one in the centre of each mortar joint between blocks, similarly to the hand-held moisture metre measurements. Additional readings of the indoor and outdoor environment are made at the time of recording each set of measurements.

The values of%WME and W were mapped with GIS on a digital elevation model of the surveyed area. To do so, the first step was obtaining a georeferenced 3D base map of the wall. A point cloud of the wall was obtained by means of monoscopic photogrammetry. 14 10.2 Mpx photographs were taken with a CCD-sensor Pentax KD10 camera. 26 8-bit coded targets were placed around the surveyed area to create a reference system. From these, a 3D 1236,702-point cloud was obtained with PhotoModeler Scanner (6.2.2.596) software. The point cloud is orientated and georeferenced by determining a datum and an origin of the coordinate system. To work with the point cloud of the wall, it is considered as if the wall was a horizontal topographic surface. Therefore, an arbitrary vertical plane is set as a horizontal datum, so that all the values in the model have a positive elevation. The origin of the coordinate system is set in one corner of the surveyed areas. In this way, each point of the cloud has X, Y, Z coordinates that will be used for relative georeferencing in GIS.

Once the point cloud is escalated and georeferenced to the local coordinate system, a topographical surface is generated from a raster surface. To do so, the data from the point cloud was converted to a shapefile (.shp) with ArcGis and a raster surface was created from the shapefile through IDW (Inverse Distance Weighted) interpolation.

Once the base map was created, each value of%WME and W is assigned to their exact point of the shapefile model so a GIS

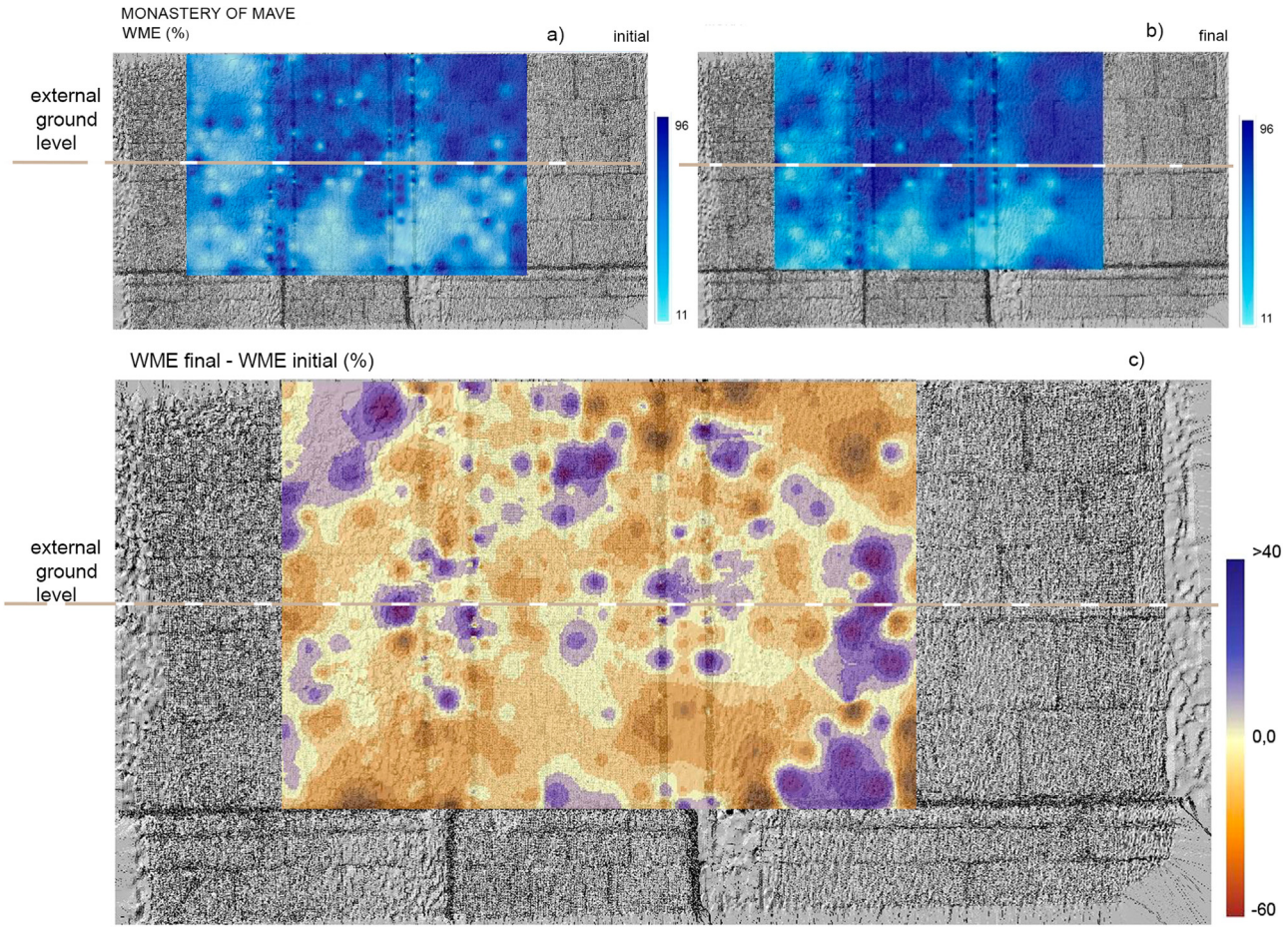

Fig. 6. Maps of Initial (a) and final (b) WME values and map subtraction (c) of WME maps performed using GIS. The initial WME map (a) is subtracted to the final WME map (b). The resulting maps are overlapped on the GIS IDW raster surface.

model, which includes the sets of measurements at different times, is generated and makes it possible to perform algebraic operations between maps.

Operating with data through GIS allows generating new sets of data from existing ones. As both high values of WME and W relate to an increase of surface moisture, a new aggregated dimensionless "moisture index" (M) is calculated as:

$$M = W + WME$$

4. Results

4.1. Electrical resistivity tomography

Fig. 4 shows the sequence of the 5 ERT profiles for the main section of the wall and the pilaster and Fig. 5 shows an example of how these profiles relate to the different sections of the studied walls. Lower resistivities correspond to moister areas, while higher resistivities relate to drier ones.

The overall average resistivity of the thinner wall sections without buttress outside nor pilaster inside is lower than the one of the thicker wall sections (with pilaster and buttress). The highest resistivity of both studied sections appears at the bottom of the pilaster sections, corresponding to the underground portion of the buttress outside. Lowest resistivities appear related to mortar joints and the indoor surface of the wall. All ERT profiles show an area of high resistivity at the external ground level. The resistivity distribution pattern does not change dramatically throughout the rain episode, although resistivity values decrease slightly, particularly in the areas associated with mortar joints.

4.2. Surface resistivity

Fig. 6a and b shows the WME maps at the beginning and at the end of the rain episode. As in the case of ERT, the overall pattern of WME does not change dramatically. However, there is an increase of the WME values throughout the test. Fig. 6c displays a map of the increment of final values of WME in relation to the initial ones calculated from subtracting both maps in GIS. This newly generated map shows a patchy distribution of the areas where WME increases. These patches are, however, distributed mainly towards the very bottom of the surveyed area and the area above the exterior ground level. The distribution of areas with increased WME also show what appears to be a fan-shaped pattern from the pilaster-buttress area downwards.

4.3. Humidity ratios (Evaporative behaviour)

Fig. 7a shows all calculated values of humidity ratio (W) against temperature for each measured point of the wall both at the initial and final stages of the survey as well as the threshold values of the outdoor humidity ratio (W_o) and the indoor humidity ratio (W_i). The outdoor humidity ratio (W_o) should represent the minimum value and is considered the reference value. The difference between these values should be considered as an indication of the overall evaporative behaviour. Hence, the "factor of intensity

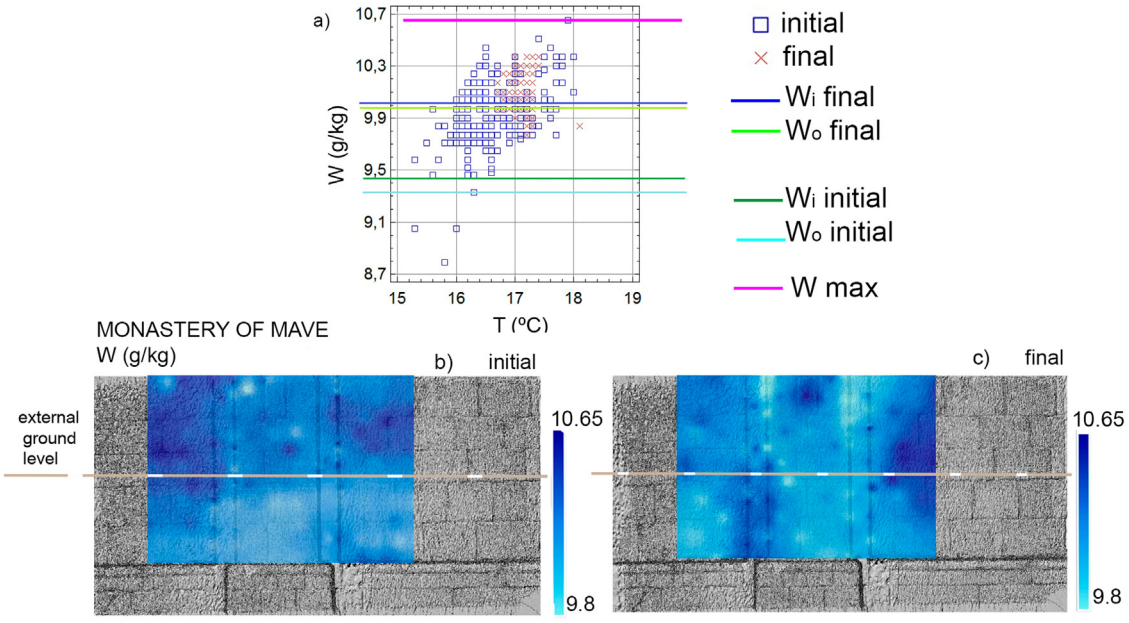

Fig. 7. Humidity ratio vs temperature graph (a) including all the measured points at the initial and the final stages of the survey. Threshold values of the outdoor (Wo final and initial) and the indoor (Wi final and initial) humidity ratio are shown as horizontal lines, as W_{max}. Values between W_{max} and minimum W_o indicate evaporation. Maps of initial (b) and final (c) humidity ratio (W) values overlapped on the IDW raster surface. Note that the scale differs between the two maps to highlight the differences in the final values of W, as these are more homogeneous than the initial ones.

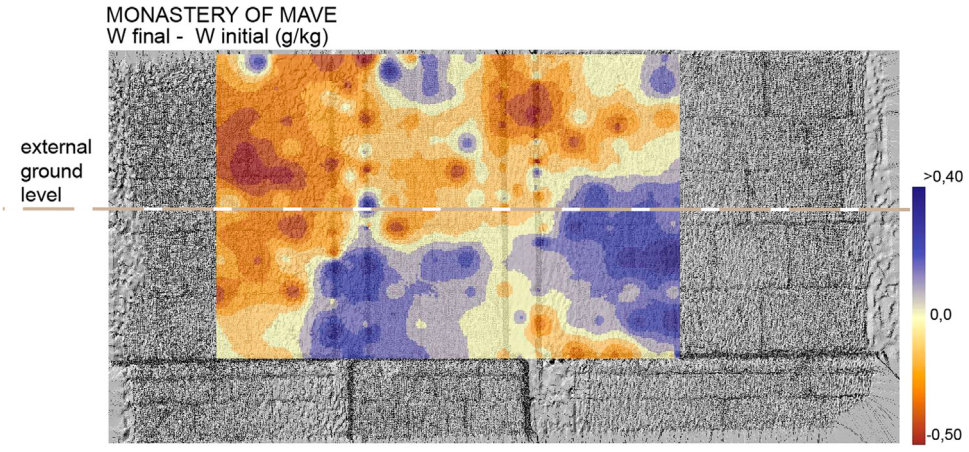

Fig. 8. Map subtraction of W maps performed using GIS. The initial W map is subtracted to the final W map. The resulting map is overlapped on the GIS IDW raster surface.

of evaporation" (F_i) is calculated as:

$$F_i = W_{max} - -W_o$$

Where W_{max} is the highest value of indoor humidity ratio (W_i) recorded on the wall. Outdoor air temperature at the beginning of the survey on day 1 was 16.2 °C and at the end of the survey on day 2 was 17.0 °C. W_o was 9.46 g/kg on day 1 and 9.97 g/kg on day 2. Indoor air temperature at the beginning of the survey on day 1 was 16.3 °C and at the end of the survey on day 2 was 16.9 °C. W_i was 9.33 g/kg for day 1 and 10.04 g/kg for day 2.

W_{max} was 10.65 g/kg on day 1 and 10.37 g/kg on day 2. Hence the maximum factor of intensity of evaporation (F_i) was 1.19 g/kg on day 1 and 0.4 g/kg on day 2.

Fig. 7b and c shows the humidity ratio (W) maps at the beginning and at the end of the rain episode and Fig. 8 shows the map of the increment of W calculated from subtracting both maps in GIS. Contrarily to the results shown by ERT and WME, the pattern of maximum evaporation points changes from the start to the end of the survey. At the end of the survey the evaporation increases significatively at the top part of the pilaster-buttress area and at the portion of the wall that corresponds to the areas below the external ground level.

4.4. Moisture index

Fig. 9 represents a map of the increment of the calculated moisture index (M, calculated by adding WME and W) from the start of the survey to the end. Positive values of this index represent areas where both surface moisture and evaporation increased.

5. Discussion

Electrical resistivity results coupled with the study of the evaporation allows interpreting moisture ingress during the studied driven rain episode. The presented data also highlight the usefulness of GIS to improve interpretations through 3D data representation and map algebra. Fig. 10a shows a detail of the bottom part of the buttress outside the surveyed area as, during rain, moisture

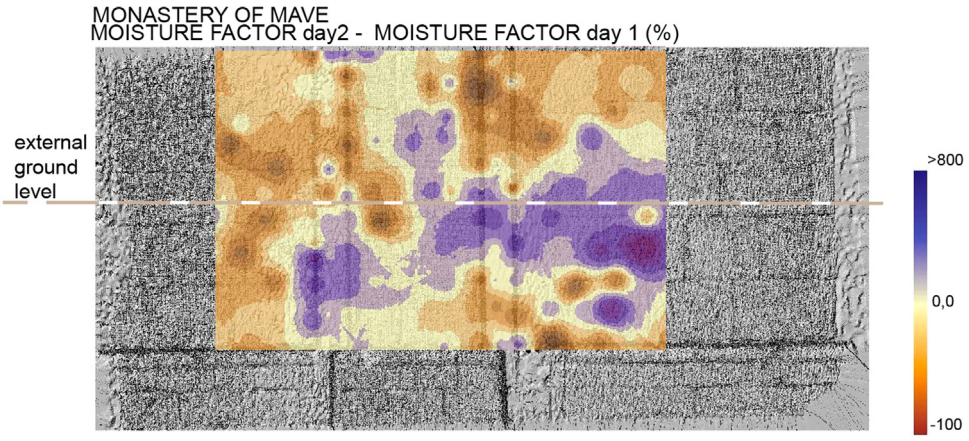

Fig. 9. Map subtraction of moisture index M maps performed using GIS. The initial M map is subtracted to the final M map. The resulting map is overlapped on the GIS IDW raster surface.

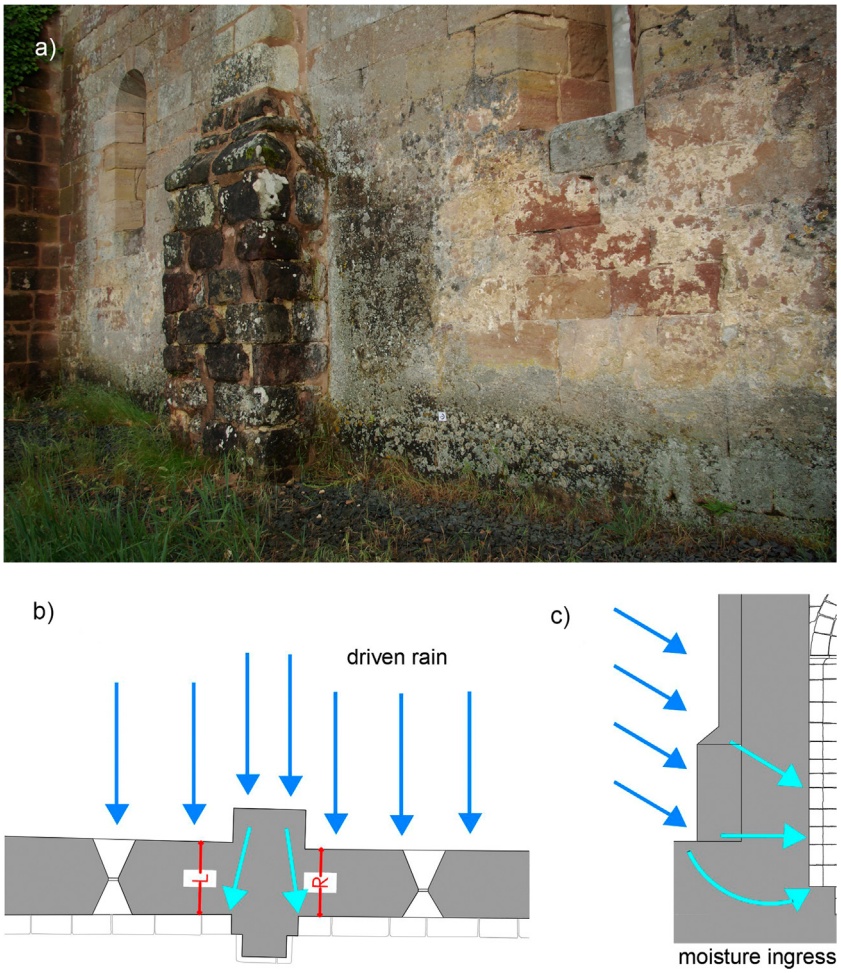

Fig. 10. View of the bottom part of the buttress outside the surveyed area (a). The horizontal section of the buttress is larger at this bottom part than at the top. The bottom part of the buttress falls outside the roof's eave action and has some sloping planes at the top that maximize the amount of driven rain impacting on the buttress. Plan (b) and elevation (c) views of the walls at the surveyed area showing moisture ingress paths through the walls.

ingress is deeply conditioned by the different thickness of the wall and the buttress-pilaster compound, as well as by the morphology of the buttress.

Moisture ingresses quickly inside the building through the thinner wall, preferably through mortar joints as shown by ERT profiles (Fig. 4). The areas of the thinner wall which are below the external ground receive some moisture due to infiltration (Fig. 4a) while the buttress-pilaster compound reduces the penetration of underground infiltration (Fig. 4b). Besides moisture accumulation, lower resistivities at the interior surface of the wall may be also related with salt accumulation and moisture retention by biological activity.

Most of the moisture during the rain episode comes from the top of the wall, particularly in the buttress-pilaster area (Figs. 6c and 8). The buttress has a larger horizontal section at the bottom part than at the top, forming sloping planes that maximize

the amount of driven rain impacting on the buttress (Fig. 10). The buttress morphology also shunts some of the rain towards the rest of the wall (as shown by the biological growth pattern visible in Fig. 10a). Thus, moisture penetrates from the top throughout the pilaster more intensely than in the rest of the wall (Figs. 8 and 9) and forms a fan-shaped pattern from the pilaster-buttress area towards the rest of the wall (Fig. 6c).

The right side of the wall (looking from the inside of the building) receives more moisture than the left side (Figs. 6-9), which may be due to the slight northeaster component of the driven rain (N11E) as well as the thinner section of the right part of the wall in relation to the left one (Figs. 1 and 10a).

6. Conclusions

This paper highlights how the usefulness of non-destructive techniques in interpreting historic building conservation issues is improved by combining several methods: in this case two different resistivity-based techniques (hand-held moisture metre and ERT) and the evaluation of evaporation (moisture ratios). Inexpensive and quick hand-held resistivity-based moisture meters complement the more expensive and time-consuming electrical resistivity tomography. The former allows mapping large areas of a building surface, while the latter permits analysing subsurface processes and, together, they make a 3D interpretation possible.

In addition to this, non-destructive techniques allow reiterating measurement and mapping over time, so a four-dimensional space (4D) [12,40] is obtained and the interpretation of dynamic processes, such as moisture ingress, is improved in relation to single snapshots of the situation of the building at a certain time.

As electrical resistivity measurements are affected by factors other than moisture, the evaluation of evaporation areas improves their interpretation. Using both techniques one can assess not only how moisture distributes but also how it interacts with the indoor environment.

The results of surface non-destructive techniques can be represented in a GIS environment considering digital elevation models of stone building surfaces as a topographic surface. GIS does not only allow creating maps that fit on 3D surfaces, but allows operating with several layers of data, either from different techniques or testing times. Presently GIS is underused in this context and Building Information Models (BIM) seem to be preferred. However, the use of GIS has the advantage over nowadays BIM of allowing algebraic operations between recorded data sets. As shown by the examples of the proposed “moisture index” and map algebra in this paper, GIS is a powerful tool to improve the interpretation of surface non-destructive techniques, particularly when using several of them.

The case study presented here shows how building features can modify deeply moisture dynamics and maximise local anisotropy, particularly in the increasingly frequent scenario of wind-driven rain. In the present case, a compound of an external tower buttress and an internal pilaster decreases moisture ingress through ground infiltration while increasing moisture retention into the wall due to its larger mass. This, in turn, multiplies the incidence of moisture-related processes inside the building.

Acknowledgements

This research was supported by Top Heritage (P2018/NMT-4372) programme from the Regional Government of Madrid (Spain) and Grants “PIC2020–116896RB-C21”, “PIC2020–116896RB-C22” funded by MCIN/AEI/ 10.13039/501100011033.

References

[1] P.M. Congedo, C. Baglivo, G. Quarta, P. Di Gloria, D. D’Agostino, Definition of a protocol for the experimental monitoring of rising damp in three different masonry models with tuff, carparo, and lecce stone, Energies 15 (2022) 892, doi:10.3390/en15030892.
[2] S. McCabe, B. Smith, C. Adamson, D.I Mullan, D. McAllister, The “greening” of natural stone buildings:quartz sandstone performance as a secondary indicator of climate change in the British isles? Atmospheric Climate Sci. 1 (2011) 165–171, doi:10.4236/acs.2011.14018.
[3] S. McCabe, P. Brimblecombe, B.J. Smith, D. McAllister, S. Srinivasan, P.A.M. Basheer, The use and meanings of ‘time of wetness’ in understanding building stone decay, Q. J. Eng. Geol. Hydrogeol. 46 (2013) 469–476, doi:10.1144/qjegh2012-048.
[4] L. Mol, H. Viles, Exposing drying patterns: using electrical resistivity tomography to monitor capillary rise in sandstone under varying drying conditions, Environ. Earth Sci. 68 (2013) 1647–1659, doi:10.1007/s12665-012-1858-x.
[5] D. D’agostino, Moisture dynamics in an historical masonry structure: the Cathedral of Lecce (South Italy), Build. Environ. 63 (2013) 122–133, doi:10.1016/j.buildenv.2013.02.008.
[6] D. McAllister, Patricia Warke, S. McCabe, M. Gomez-Heras, Evaporative moisture loss from heterogeneous stone: material-environment interactions during drying, Geomorphology 273 (2016) 308–322, doi:10.1016/j.geomorph.2016.08.008.
[7] Z.L. Zhou, X. Cai, D. Ma, L. Chen, S. Wang, L.H. Tan, Dynamic tensile properties of sandstone subjected to wetting and drying cycles, Constr. Build. Mater. 182 (2018) 215–232, doi:10.1016/j.conbuildmat.2018.06.056.
[8] C. Alves, C.A.M. Figueiredo, J. Sanjurjo-Sanchez, A.C. Hernandez, Effects of water on natural stone in the built environment - a review, Geosciences 11 (2021) 459, doi:10.3390/geosciences11110459.
[9] E. Rosina, A. Sansonetti, N. Ludwig, Moisture: the problem that any conservator faced in his professional life, J. Cult. Herit. 31 (2018) S1–S2 Supplement, doi:10.1016/j.culher.2018.04.022.
[10] D. Camuffo, Standardization activity in the evaluation of moisture content, J. Cult. Herit. 31 (2018) S10–S14 Supplement, doi:10.1016/j.culher.2018.03.021.
[11] E. Rosina, When and how reducing moisture content for the conservation of historic building. A problem solving view or monitoring approach? J. Cult. Herit. 31 (2018) S82–S88 Supplement, doi:10.1016/j.culher.2018.03.023.
[12] L. Lopez-Gonzalez, R. Otero de Cosca, M. Gomez-Heras, S. Gonzalez Morales, A 4D GIS methodology to study variations in evaporation points on a heritage building, Environ. Earth Sci. 75 (2016) 1113, doi:10.1007/s12665-016-5907-8.
[13] C. Lerma, Á. Mas, E. Gil, J. Vercher, M.J. Peñalver, Pathology of building materials in historic buildings. Relationship between laboratory testing and infrared thermography, Mater. Construcc 64 (2014) e009, doi:10.3989/mc.2013.06612.
[14] R. Vecchiattini, Moisture monitoring experience in the old town of Genoa (Italy), J. Cult. Herit. 31 (2018) S71–S81 Supplement, doi:10.1016/j.culher.2018.04.007.
[15] O. Sass, H.A. Viles, Two-dimensional resistivity surveys of the moisture content of historic limestone walls in Oxford, UK: implications for understanding catastrophic stone deterioration. Limestone in the built environment, Geological Soc. (2010) 237–249, doi:10.1144/SP331.22.
[16] O. Sass, H.A. Viles, Wetting and drying of masonry walls: 2D-resistivity monitoring of driving rain experiments on historic stonework in Oxford, UK, J. Appl. Geophys. 70 (2010) 72–83, doi:10.1016/j.jappgeo.2009.11.006.
[17] S.A. Orr, L. Fusade, M. Young, D. Stelfox, A. Leslie, H.Viles J.Curran, Moisture monitoring of stone masonry: a comparison of microwave and radar on a granite wall and a sandstone tower, J. Cult. Herit. 41 (2020) 61–73, doi:10.1016/j.culher.2019.07.011.
[18] J. Válek, S. Kruschwitz, J. Wöstmann, T. Kind, J. Valach, C. Köpp, J. Lesák, Non-destructive Investigation of Wet Building Material: multimethodical Approach, J. Perform. Constr. Facil. 24 (2010) 462–472, doi:10.1061/(ASCE)CF.1943-5509.0000056.
[19] M.I. Martínez-Garrido, R. Fort, M. Gómez-Heras, J. Valles-Iriso, M.J. Varas-Muriel, A comprehensive study for moisture control in cultural heritage using non-destructive techniques, J. Appl. Geophy. 155 (2018) 36–52, doi:10.1016/j.jappgeo.2018.03.008.
[20] C. Lerma, J.G. Borràs, A. Mas, M.E. Torner, J. Vercher, E. Gil, Evaluation of hygrothermal behaviour in heritage buildings through sensors, CFD modelling and IRT, Sensors 21 (2021) 566, doi:10.3390/s21020566.
[21] L. Mol, P.R. Preston, The writing’s in the wall: a review of new preliminary applications of electrical resistivity tomography within archaeology, Archaeometry 52 (2010) 1079–1095, doi:10.1111/j.1475-4754.2010.00516.x.
[22] P. Tsourlos, G.N. Tsokas, Non-destructive electrical resistivity tomography survey at the south walls of the acropolis of athens, Archaeol. Prospect. 18 (2011) 173–186, doi:10.1002/arp.416.
[23] E. Cardarelli, G. De Donno, C. Scatigno, I. Oliveti, M. Preite Martinez, N. Prieto-Taboada, Geophysical and geochemical techniques to assess the origin of rising damp of a Roman building (Ostia Antica archaeological site), Microchem. J. 129 (2016) 49–57, doi:10.1016/j.microc.2016.06.006.
[24] G. De Donno, L. Di Giambattista, L. Orlando, High-resolution investigation of masonry samples through GPR and electrical resistivity tomography, Constr. Build. Mater. 154 (2017) 1234–1249, doi:10.1016/j.conbuildmat.2017.06.112.
[25] H. Forsén, V. Tarvainen, Accuracy and functionality of hand held wood moisture content meters, VTTpublications num 420 (2000) 95 ISBN 951-38-5581-3.

[26] K. Wilhelm, H. Viles, Ò. Burke, The influence of salt on handheld electrical moisture meters: can they be used to detect salt problems in porous stone? Int. J. Architect. Heritage 10 (6) (2016) 735–748, doi:10.1080/15583058.2015.1109733.
[27] D. Camuffo, Microclimate for Cultural Heritage, Elsevier, 2014.
[28] M. Danese, D. Gioia, M. Biscione, Integrated methods for cultural heritage risk assessment: google earth engine, spatial analysis, machine learning, Computational Science and Its Applications – ICCSA, Springer, Cham, 2021 ICCSA 2021. Lecture Notes in Computer Sciencevol 12951, doi:10.1007/978-3-030-86970-0_42.
[29] Y. Fujii, T. Shogaki, M. Miyakawa, Photogrammetric documentation and non-invasive investigation of a stone dry dock, the Yokosuka Arsenal dry dock, Japan, Eng. Geol. 234 (1) (2018) 122–131, doi:10.1016/j.enggeo.2017.12.022.
[30] M. Gomez-Heras, J.A. Ortega-Becerril, Julio Garrote, Rafael Fort and Laura Lopez-Gonzalez Morphometric measurements of bedrock rivers at different spatial scales and applications to geomorphological heritage research, Prog. Earth Planet Sci. 6 (2019) 29, doi:10.1186/s40645-019-0275-0.
[31] L. Mol, L. Clarke, Integrating structure-from-motion photogrammetry into rock weathering field methodologies, Earth Surf. Process. Landforms. 44 (2019) 2671–2684, doi:10.1002/esp.4693.
[32] M. Arce-Recatalá, S. García-Morales, N. Van den Bossche, Quantifying wind-driven rain intrusion – a comparative study on the water management features of different types of rear-ventilated facade systems, E3S Web Conf. 172 (2020) 23007, doi:10.1051/e3sconf/202017223007.
[33] J. Martínez-Martínez, A. Abellán, E. Berrezueta, Erosion directionality and seasonality study using the anisotropy matrix, Sci. Total Environ. 804 (2022) 150165, doi:10.1016/j.scitotenv.2021.150165.
[34] J. Perez-Bella, J. Domínguez-Hernández, B. Sordíguez-Soria, J.J. del Coz-Díaz, E. Cano-Suñén, Estimation of the exposures of buildings to driving rain in Spain from daily wind and rain data, Build. Environ. 57 (2012) 259–270, doi:10.1016/j.buildenv.2012.05.010.
[35] S.A. Orr, M. Young, D. Stelfox, J. Curran, H. Viles, Wind-driven rain and future risk to built heritage in the United Kingdom: novel metrics for characterising rain spells, Sci. Total Environ. 640–641 (2018) 1098–1111, doi:10.1016/j.scitotenv.2018.05.354.
[36] S. Fatoric, E. Seekamp, Are cultural heritage and resources threatened by climate change? A systematic literature review, Clim. Change 142 (2017) 227–254, doi:10.1007/s10584-017-1929-9.
[37] J. Nuño González, A. Tovar Nuñez, P. Moro Simón, Análisis De Las Fases construidas. Monasterio de Santa María De Mave. Plan de Intervención Del Románico Norte, Fundación Santa María la Real, 2007.
[38] F. Wenner, A method for measuring earth resistivity, J. Franklin. Inst. 180 (1915) 373–375, doi:10.1016/s0016-0032(15)90298-3.
[39] S. García Morales, L. López-González, A. Collado Gómez, Metodología de inspección higrotérmica para la determinación de un factor intensidad de evaporación en edificios históricos, Inf. Constr. 64 (2012) 69–78, doi:10.3989/ic.11.073.
[40] L. Bertolla, J.L. Porsani, F. Soldovieri, I. Catapano, GPR-4D monitoring a controlled LNAPL spill in a masonry tank at USP, Brazil, J. Appl. Geophy. 103 (2014) 237–244, doi:10.1016/j.jappgeo.2014.02.006.